4 NONLINEAR OPTICAL PROPERTIES OF SEMICONDUCTOR QUANTUM WELLS

D. S. Chemla and D. A. B. Miller

AT & T BELL LABORATORIES
HOLMDEL, NEW JERSEY

S. Schmitt-Rink

AT & T BELL LABORATORIES
MURRAY HILL, NEW JERSEY

I. INTRODUCTION

The concept of excitons has been in existence for over fifty years, and it is a key concept in the physics of the optical properties of semiconductors. Two developments over the past few decades have opened up new areas of the

OPTICAL NONLINEARITIES AND INSTABILITIES IN SEMICONDUCTORS

ISBN 0-12-332915-9

physics of excitons in semiconductors. The technology of lasers enables us to generate controlled densities of excitons and electron–hole pairs to see the many-body effects of these particles on each other through the changes that they induce in the optical properties. Furthermore, the short-pulse optical techniques that have recently become available allow the dynamics of these particles to be observed with temporal resolution comparable to the elementary time scales of the particles, such as the phonon-scattering times and the orbit times of the excitons themselves. The second development has been the technology of layered semiconductor growth, which is now able to grow structures at will with atomic monolayer precision. Among the many uses of this growth technology is the ability to generate structures that can confine excitons in dimensions less than the usual Bohr radius of the exciton. Although one might expect at first sight that this gross interference with the exciton would destroy it, in fact, the opposite is true. The resulting excitons are actually so robust that clear excitonic absorption resonances can be seen at room temperature, a fact that actually makes them easier to study than bulk excitons.

The combination of lasers and layered structures for studying exciton physics is barely five years old, and it is primarily this rapidly evolving field that is the subject of this chapter. We shall discuss the physics of excitons and the resulting linear optical absorption in quantum wells (QWs) before going on to the changes induced by optically generated exciton and electron–hole pair populations. Finally, we shall consider the effects of virtual populations of excitons. The emphasis will be on the physics of these processes, presented in an intuitive fashion as far as possible, rather than on complete, rigorous treatments or historical reviews of the literature. The article is self-contained as far as possible, although we have attempted to make it complementary in emphasis to the chapter by Miller et al. For a larger perspective on active research in optical properties of quantum wells, the reader is referred to the recent collection of articles (Chemla and Pinczuk, 1986).

II. EXCITON STATES IN SEMICONDUCTOR QUANTUM WELLS

In semiconductor QWs, the electrons (e) and holes (h) are free to move in the plane of the layers (x, y) and their motion normal (z) to the layers is controlled by the potential discontinuities at the interfaces (Dingle et al., 1974). It has been shown that the single-particle states are well described

within the effective mass approximation (EMA). The wave functions are plane waves for the in-plane motion. The quantization normal to the layers gives "particle in a box" wave functions, which are sinusoidal in the well and exponential outside. The low-energy states form a discrete set of two-dimensional (2D) valence (v) and conduction (c) subbands with a steplike density of states. These states can be labeled by a "normal motion" quantum number $n_z = 1, 2, \ldots$. The states with energy above the band discontinuities form three-dimensional (3D) continua with a density of states presenting resonances at specific energies (Bastard, 1984). The nature of these single-particle states is discussed in more detail in chapter 13. In order to discuss the absorption spectra, we need to know how e–h pair states are constructed from these single-particle states, and this is briefly discussed in this section.

QWs have properties intermediate between 2D and 3D material; it is therefore instructive first to compare excitonic effects in pure 2D and 3D before discussing the influence of the finite well thickness. The theory of excitons (x) in 3D semiconductors is extremely well documented (Elliot, 1957). It turns out that, within the EMA, it can be easily extended to Wannier excitons with a pure 2D motion and $1/r$ e–h attraction (Shinada and Sugano, 1966).

Let us consider first the ideal case of a semiconductor of band gap E_g with two isotropic valence and conduction bands with masses $m_v = -m_h$ and $m_c = m_e$, respectively. Throughout this chapter, we shall use as units of energy and length the 3D Rydberg and Bohr radius, respectively, $R_0 = e^4\mu/2\epsilon_0^2\hbar^2$ and $a_0 = \epsilon_0\hbar^2/\mu e^2$, where $\mu^{-1} = m_e^{-1} + m_h^{-1}$ is the reduced e–h mass and ϵ_0 the dielectric constant. The solution of the 2D Schroedinger equation gives a series of bound states with energies $E_n^{2D} = E_g - R_0/(n - 1/2)^2$ as compared to the 3D result $E_n^{3D} = E_g - R_0/n^2$. The wave function of the 1s state in real space is

$$U_{1s}^{2D}(r) = \left(\frac{2}{\pi}\right)^{1/2} \frac{2}{a_0} \exp\left(-\frac{2r}{a_0}\right) \tag{1a}$$

and in momentum space

$$U_{1s}^{2D}(k) = \frac{(2\pi)^{1/2} a_0}{\left[1 + (a_0 k/2)^2\right]^{3/2}} \tag{1b}$$

Let us recall for comparison that in 3D, these functions are

$$U_{1s}^{3D}(r) = \frac{1}{(\pi)^{1/2} a_0^{3/2}} \exp\left(-\frac{r}{a_0}\right) \tag{2a}$$

and

$$U_{1s}^{3D}(k) = \frac{(8\pi)^{1/2} a_0^{3/2}}{\left[1 + (a_0 k)^2\right]^2} \tag{2b}$$

In 2D, the 1s exciton binding energy and Bohr radius are $R_{2D} = 4R_0$ and $a_0/2$, respectively, and the maximum radial charge density occurs at $a_{2D} = a_0/4$. Furthermore, the probability of finding the e and h in the same unit cell varies like $|U_n^{2D}(r = 0)|^2 = (2n - 1)^{-3}|U_{1s}^{2D}(r = 0)|^2$, whereas in 3D, $|U_n^{3D}(r = 0)|^2 = (n)^{-3}|U_{1s}^{3D}(r = 0)|^2$, which shows that the e–h correlation in excited bound states decreases more rapidly in 2D than in 3D. Much the same can be said for the scattering states (i.e. the unbound electron–hole pair states). In 2D, one finds

$$|U_k^{2D}(r = 0)|^2 = \frac{2}{\left[1 + \exp(-2\pi/a_0 k)\right]} \tag{3a}$$

where $a_0 k = [(E - E_g)/R_0]^{1/2}$ is the dimensionless e–h relative momentum. In 3D,

$$|U_k^{3D}(r = 0)|^2 = \frac{2\pi/a_0 k}{\left[1 - \exp(-2\pi/a_0 k)\right]} \tag{3b}$$

Real semiconductor QWs have a finite thickness and depth, and one faces many complications. The motion normal and in the plane of the layer are coupled by the Coulomb interaction. Because of the penetration of the wave functions into the barrier medium, the differences of the valence and conduction band effective masses inside and outside the well have to be accounted for. Finally, in III–V compounds, the hole motion in the plane is complex because the degeneracy of the light (lh) and heavy hole (hh) bands at the Γ point is lifted giving rise to two series of subbands. Away from $k = 0$, these subbands couple (Chang and Schulman, 1983) and acquire a highly nonparabolic dispersion so that a constant effective mass can no longer be defined for the holes (Broido and Sham, 1986). Several approximations must be made to make the problem tractable (Lee and Lin, 1979; Miller et al., 1981; Bastard et al., 1982; Greene et al., 1984).

First, the coupling among the various subbands and light and heavy holes is neglected. This is justified as long as the energy separation between the subbands is much larger than the exciton binding energy. Since excitons are built up from a linear combination of free e–h states distributed according to U_{1s}, the valence subband dispersion is averaged to give a "mean effective mass" for the holes. The value of this mass in the literature is quite often a

matter of personal taste. Finally, variational procedures are used, starting from well-behaved wave functions, to solve the exciton Schroedinger equation. The main results are the following. For a trial wave function inseparable in $z_{e,h}$ and $(x, y)_{e,h}$ and infinitely deep wells, a smooth variation of the 1s exciton binding energy from $4R_0$ to R_0 is found for L_z/a_0 varying from 0 to ∞, in good agreement with physical intuition (Miller et al., 1981; Bastard et al., 1982). Unfortunately, this situation does not correspond to real QWs because in the limit of very thin wells, the wave function penetrates more and more in the barrier medium as a result of the finite confining potential, and the exciton becomes less and less confined. As $L_z \to 0$, the exciton tends toward the 3D exciton of this material and the binding energy toward the corresponding Rydberg (Greene et al., 1984). Thus, the enhancement of the binding energy shows an optimum $< 4R_0$ for narrow but finite QWs.

In order to gain physical insight into real QW excitons, it is desirable to have a reasonably good exciton ground state wave function in a closed form. For narrow QWs, the confinement energy is much larger than the binding energy and one can assume that the motion along z is governed by the QW potential discontinuity only. It is then possible in the variational calculation to use as a trial wave function the separable form $\phi_e(z_e)\phi_h(z_h)U_{1s}^{2D}(r)$, where $\phi_{e,h}(z_{e,h})$ are the $n_z = 1$ single-particle wave functions in the z direction and $U_{1s}^{2D}(r)$ has the same functional form as in Eq. 1a, with a variational radius parameter a_{2D} being used instead of $a_0/4$. This approach gives results comparable to more sophisticated theories (Miller et al., 1985). In the case of 100 Å GaAs/AlGaAs QWs it is found that $a_{2D} \sim 65$ Å and $R_{2D} \sim 9$ meV, as compared to $a_0 \sim 140$ Å and $R_0 \sim 4.2$ meV. If one accounts for the small penetration of the wave function into the barrier material, approximately 20 Å, the charge distribution is like a slightly oblate spheroid with nevertheless a substantial reduction in the average e–h separation (as measured by a_{2D}), which is responsible for the increased binding energy.

One can even go one step further and replace ϕ_e and ϕ_h by the single-particle wave functions of an infinite well of somewhat larger adjusted thickness. This accounts approximately for the penetration into the barrier medium and is mathematically the simplest trial wave function that can be chosen while still preserving the principle features of the actual exciton state (Miller et al., 1985).

In summary, in the pure 2D case, the exciton ground state binding energy is four times larger than in 3D and the relative motion wave function forms a flat disk with a radial charge density maximum at $a_{2D} = a_0/4$ rather than

at a_0 as in 3D. The excited states are more separated from the ground state than in 3D and, correspondingly, the probability of finding the e and h in the same unit cell decreases more rapidly. In real QWs, the situation is intermediate between the 2D and 3D limits. Although the exciton conserves a rather isotropic charge distribution, the relative separation between the electron and hole in the 1s state is substantially reduced as compared to 3D. This results in a binding energy and a probability of finding the e and h in the same unit cell that is considerably larger than in 3D. In addition, in III–V materials, the light and heavy holes can give distinct exciton states.

III. LINEAR ABSORPTION IN SEMICONDUCTOR QUANTUM WELLS

In QWs, as in 3D semiconductors, the optical spectra near the band gap energy are profoundly influenced by the e–h correlation that induces excitonic resonances below the gap and enhancement above. In fact, it has been found experimentally that excitonic effects are strongly enhanced in the absorption spectra of QWs (Dingle et al., 1974; Chemla, 1983, 1985; Chemla and Miller, 1985; Miller and Kleinman, 1985). This is due to the combination of several factors discussed in the previous section. In this section we shall briefly present the main results obtained on the linear excitonic optical absorption in semiconductor QWs.

In bulk semiconductors, the optical absorption spectrum is proportional to the atomic transition probability, as modified by the probability of finding the e and h in the same unit cell. The imaginary part of the optical susceptibility χ_{3D} is formally given by

$$\operatorname{Im} \chi_{3D} = 2\pi |er_{cv}|^2 \sum_n |U_n^{3D}(r = 0)|^2 \, \delta\left(\hbar\omega - E_n^{3D}\right) \tag{4a}$$

where er_{cv} is the atomic dipole matrix element, and $U_n^{3D}(r)$ the envelope wave function of the e–h relative motion, E_n^{3D} being the corresponding pair energy. Here, n runs both over bound and scattering states.

In QWs, χ is strictly a nonlocal function in real space, but for L_z much less than the wavelength of the light, a suitably averaged susceptibility can be defined (Miller et al., 1986a). For infinitely deep wells, the e and h single-particle wave functions are orthonormal, and the spatial average of χ over the QW yields the selection rule that optical transitions can only take place between valence and conduction subbands having the same quantum number n_z. The Coulomb interaction couples the various transitions, which

among other things gives rise to a Fano lineshape of excitons associated with excited subbands. In narrow QWs, in which the wave functions are consequently approximately separable, one can ignore this subtlety; each transition has its own exciton series

$$\operatorname{Im} \chi_{2D} = 2\pi |er_{cv}|^2 \sum_n |U_n^{2D}(r=0)|^2 \, \delta\left(\hbar\omega - E_n^{2D}\right)/L_z \qquad (4b)$$

where $U_n^{2D}(r)$ is the associated in-plane relative motion wave function.

In reality, the e and h tunnel by different amounts into the barriers, which leads to small but finite transition probabilities for the "forbidden transitions," i.e. those transitions for which the wave functions would otherwise be orthogonal. If an asymmetry is introduced, for example by applying an electric field, all of these transitions become partly allowed and are clearly observed (Miller et al., 1986a, b). (See also chapter 13 for a discussion).

In III–V compounds, because of the heavy and light hole mixing away from $k = 0$, one can even observe transitions that are normally parity forbidden at the microscope level (Chang and Schulman, 1983). The angular momentum selection rules for the interband matrix element show that for transitions from $k = 0$ heavy and light hole states to $k = 0$ conduction band states, the $|r_{cv}|^2$ are in a ratio 3/4 and 1/4 for optical fields polarized parallel to the layers, and 0 and 1 for orthogonal polarization. In doped or laser-excited QWs, the Coulomb interaction couples states with different momentum k, so that this rule is lifted (Sooryakumar et al., 1985; Ruckenstein et al., 1986).

At low temperatures, exciton resonances are clearly observed at the onset of each interband transition, the light and heavy hole doublet being well resolved at least in the lowest transitions. At the onset of continuum absorption, above the band gap discontinuity, delocalized exciton resonances were resolved by resonant Raman scattering and a weak structure was also seen in absorption (Zucker et al., 1984b).

The exciton lines in QWs are broad compared to other exciton lines at low temperature. The majority of the broadening has been identified as due to the unavoidable fluctations in the QW thickness (Weisbuch et al., 1981) and is therefore an inhomogeneous broadening. The best samples have interfaces with an islandlike structure with steps one monolayer high. The lateral correlation length depends on the details of the growth conditions; it is usually of the order of several hundred Å. This results in potential fluctuations seen by the excitons that produce very interesting localization effects both in linear and in nonlinear optics (Hegarty and Sturge, 1985;

Takagahara and Hanamura, 1986). The inhomogeneous line width increases as the thickness of the QW decreases; a typical value of the line width at half maximum is ~ 2 meV for 100 Å GaAs–AlGaAs QWs. Information on the homogeneous line width that underlies the dominant inhomogeneous broadening has been obtained by resonant Rayleigh (Hegarty and Sturge, 1985) and Raman (Zucker et al., 1987) scattering; it can be as narrow as 0.1 meV in GaAs–AlGaAs QWs. The line broadening can be accounted for in Eq. 4b by replacing the Dirac functions by phenomenological profiles with a finite width.

Below-gap absorption has been investigated in GaAs–AlGaAs QWs using a sensitive nonlinear optical technique that will be discussed in Section IV.B. It was found that just below the $n_z = 1$ hh-exciton peak, the absorption drops exponentially in agreement with Urbach's rule (Von Lehmen et al., 1986a). The steepness is comparable to that obtained for bulk GaAs. At low temperatures, LO phonon-assisted transitions are observed (Von Lehmen et al., 1987). About 30 meV below the $n_z = 1$ hh-exciton, the residual absorption can be as low as 10 cm^{-1} at room temperature and 0.1 cm^{-1} at 77 K.

A most remarkable property of III–V QW structures is the persistence in the absorption spectrum of well-resolved exciton resonances at room temperature and even higher (Miller et al., 1982a, b; Weiner et al., 1985a). An example of the GaAs–AlGaAs QW room temperature absorption spectrum is shown in Fig. 1. The spectrum is remarkably clear. The three $n_z = 1$, 2 and 3 plateaus are well resolved with exciton resonances at the onset of each. Similar spectra have been observed in wave guides containing a single QW (Weiner et al., 1985b). Using these structures, selection rules for light polarized parallel and perpendicular to the layers have been investigated. It was found that, within the experimental accuracy, the measured ratios of the transition strengths are in good agreement with those predicted by angular momentum theory.

The enhanced exciton oscillator strength that accompanies the larger binding energy plays a very important role in these results. However, alone it is not sufficient to explain the observations; other semiconductors have excitons more tightly bound than III–V QWs and yet their resonances disappear long before room temperature. In 3D, the exciton binding energy, through its dependence on the dielectric constant and the effective masses, scales roughly as the band gap. The dominant exciton–phonon interaction in polar semiconductors is that with LO phonons (Liebler et al., 1985) and its strength, through the dependence on the ionicity, also scales approxi-

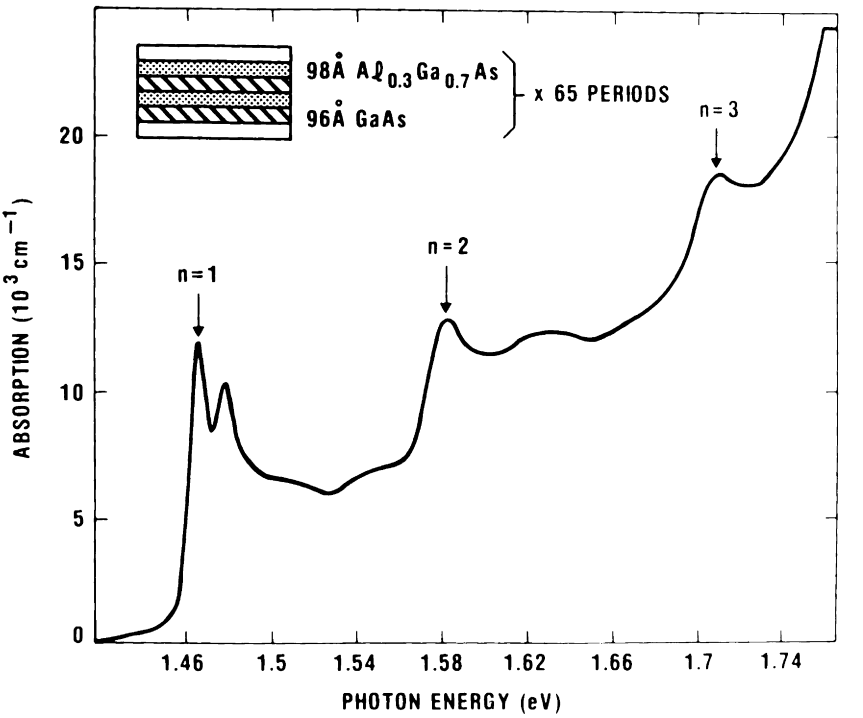

Figure 1. Room temperature absorption spectrum showing the $n_z = 1$, 2 and 3 exciton resonances and flat continua. At the fundamental edge, the heavy and light hole excitons are resolved. Between the $n_z = 1$ and $n_z = 2$ resonances, a weak structure due to a "forbidden transition" can be seen.

mately with the band gap. Thus, in 3D materials, increasing the exciton binding energy also increases the exciton sensitivity to thermal broadening and exciton resonances are only seen at low temperatures almost regardless of band gap energy. In QWs, the increased binding energy results from the artificial reduction of the e–h separation by the confinement in the QW, without any significant change of the coupling to LO phonons, as shown by resonant Raman-scattering studies (Zucker et al., 1983, 1984a). Thus, for QW excitons, the dominant mechanism for thermal broadening is essentially not modified. This was confirmed by studies of the temperature broadening of the exciton peak in GaAs–AlGaAs (Miller et al., 1982b) and GaInAs–AlInAs (Weiner et al., 1985a) QWs. It was found that the line width varies as the sum of a constant inhomogeneous term Γ_{inh} and a term

proportional to the number of LO phonons

$$\Gamma(T) = \Gamma_{inh} + \frac{\Gamma_{LO}}{\left[\exp\left(\frac{\hbar\omega_{LO}}{k_B T}\right) - 1\right]} \tag{5}$$

The parameter Γ_{LO}, which describes the strength of the interaction with LO phonons in GaAs–AlGaAs QWs ($\Gamma_{LO} \sim 5$ meV), is smaller than but comparable to that in the bulk ($\Gamma_{LO} \sim 8$ meV). This shows that the efficiency of collisions with LO phonons is hardly changed. Absorption profiles such as that of Fig. 1 are very well fitted around the lowest transitions by two Gaussian lines at the heavy and light hole resonances and a phenomenologically broadened continuum (Chemla et al., 1984).

At high temperatures, excitons are unstable against collisions with thermal phonons. In fact, in GaAs–AlGaAs QWs the LO phonon energy ($\sim$ 36 meV) is much larger than the exciton binding energy ($\sim$ 9 meV). Thus, a single exciton–LO-phonon collision can ionize the exciton and release a free e–h pair with a substantial excess energy. If the temperature broadening of the exciton resonance is interpreted as a lifetime reduction due to thermal LO-phonon scattering, it is found that at room temperature, excitons live only $\sim$ 0.4 ps in GaAs–AlGaAs and $\sim$ 0.3 ps in GaInAs–AlInAs QWs. Simple thermodynamic arguments show that the excitons have a very small probability of recovering. Consequently, at room temperature, a photon absorption process can be pictured as

$$\hbar\omega \rightarrow x \rightarrow e - h \tag{6}$$

As we shall see later, this sequence includes interesting dynamics in the nonlinear optical response of QWs.

IV. EXPERIMENTAL AND THEORETICAL INVESTIGATIONS OF NONLINEAR OPTICAL EFFECTS

The basic mechanisms responsible for the nonlinear response of semiconductors are different depending on whether virtual or real excited-state populations are generated. Excitations below and above the absorption edge have to be clearly distinguished. Before presenting particular results, it is useful to discuss these mechanisms in very broad terms.

In the case of virtual transitions induced by excitation well below the absorption edge, the electric field of the coherent laser beam induces a coherent polarization that persists only as long as the field is applied. The

nonlinear polarization can couple various optical fields, which exchange photons via the material, but no energy is deposited in the latter. During the application of the field, the state of the sample is a coherent superposition of excited states. The coherently driven components have exactly the same properties as if they were actually populated although they do not participate in any relaxation process; if they did relax by any collisions, their quantum-mechanical phase would be disturbed, they would no longer be coherent with the other components, and as far as the driving field is concerned, the associated photons would have been absorbed in real transitions. By a simple application of the uncertainty principle, the amount of time the photons spend in the excited state is $\sim \hbar/\Delta E$, where ΔE is the difference between the photon energy and the excited state energy. As long as this time is short compared to the scattering time τ_s of the excited state, the transitions will be predominantly virtual. Virtual transitions are therefore only favored under off-resonance excitation (i.e. large ΔE). The field-induced optical nonlinearities are usually small because of the large differences ΔE between the photon energies and the absorption edge; however, they are extremely fast ($\sim \hbar/\Delta E$).

Excitation above the absorption edge generates predominantly real excited-state populations with no particular quantum-mechanical coherence; this is because there are many states within ΔE of the photon energy that are consequently strongly absorbing and also strongly scattered. Because of the strong absorption, however, such above-gap excitation produces large excited-state populations for a given excitation intensity, and hence large changes in the optical properties of the material although these changes are incoherent with each other and with the driving field. These populations have a finite lifetime and participate in a number of relaxation processes. The changes they induce in the optical spectra persist as long as the populations themselves. For the specific case of semiconductors, the excited e–h states can form bound (excitons, trions, biexcitons) or unbound (e–h plasma) states, which produce different effects (Haug and Schmitt-Rink, 1984). Furthermore, ultrafast photogeneration can produce nonthermal distributions of these states. Two relaxation times should be distinguished. The first is the time it takes the excited e and h to reach a thermodynamic equilibrium among themselves (usually a fraction of a ps), and the second one is the time it takes them to equilibrate with the lattice (in the ps range). Optical transients can occur if excited species transform into one another during relaxation. For example, excitons that are generated by resonant excitation within the absorption peak are only stable at low temperatures, where they can last as long as several nanoseconds. In the case of QWs at

room temperature, they are unstable and very quickly transform into free e–h pairs. Because the two species have different effects on the optical spectra, it is necessary to distinguish among them experimentally and theoretically.

In this section, we shall review the experimental and theoretical investigations of excitonic nonlinearities in QWs. We shall then distinguish between plasma, exciton and field-induced effects. Experimentally, field effects are produced by excitation well below the absorption edge and plasma effects by excitation above it. At room temperature, exciton effects are more difficult to select; not only resonance excitation must be used but they must be observed in times short compared to the exciton ionization time. This requires femtosecond spectroscopic techniques.

The experimental method most widely used is the "pump and probe" technique, in which a strong pump beam is applied to the sample and a weak test beam is used to probe the excited sample. Measuring the transmitted test beam provides information on the absorption and gain of the sample. It is also possible to measure the photons diffracted by interference between the pump and test beam in directions different from that of the incident beams. The diffraction efficiency provides information both on the change of refractive index and absorption. These techniques have been extensively discussed in the literature (Chemla et al., 1984).

A. Nonlinear Optical Effects Induced by Thermalized Plasmas

We consider first the experiments in which an optically created real and thermalized e–h plasma is responsible for the changes in optical properties. The plasma can be generated either directly above the gap (Chemla et al., 1984) or indirectly following exciton creation by resonant absorption (Miller et al., 1982b) or LO phonon-assisted absorption (Von Lehmen et al., 1986a, 1987). For thermalization to be completed, observation must take place a few ps after excitation.

It is found experimentally that the changes in the absorption spectrum do not depend on the excitation wavelength or on its duration. They depend only on the density N of excited pairs. A typical example of the modification of the absorption spectrum as a function of the pair density is presented in Fig. 2 for GaAs–AlGaAs QWs and N between ~ 0 and $\sim 2 \times 10^{12}$ cm^{-2}. In the particular case of this set of spectra, the sample was excited with a 100 fs pump pulse about 60 meV above the hh-exciton resonance and was probed several ps later by a broadband test continuum.

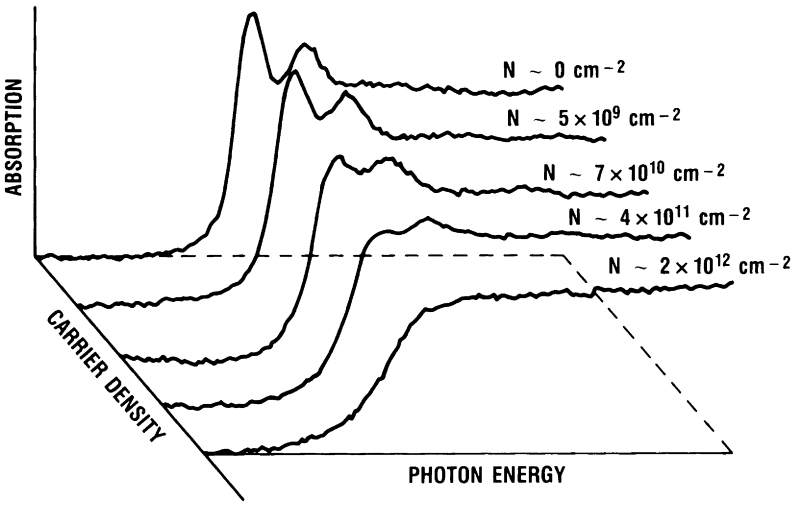

Figure 2. Absorption spectra for free e–h pair densities N between ~ 0 and $\sim 2 \times 10^{12}$ cm^{-2}, measured after thermalization of the e–h plasma.

A very smooth evolution is seen; the two exciton resonances weaken and are progressively replaced by a steplike edge. The independence of the nonlinear absorption on the excitation wavelength and thus on the way the e–h plasma is created is clearly demonstrated in Fig. 3. Here, two differential transmission spectra (absorption without pump minus absorption with pump) are compared. They were measured about 2 ps after selective exciton generation by resonant pumping (full line) and direct e–h plasma generation by nonresonant pumping (dotted line). The pump intensities were adjusted to produce the same density of pairs. Within the experimental accuracy the two curves are not distinguishable.

The changes of the optical spectra are interpreted as follows (see also Section IV.B) (Löwenau et al., 1982; Haug and Schmitt-Rink, 1984, 1985; Schmitt-Rink et al., 1984, 1985, 1986; Schmitt-Rink and Ell, 1985; Schmitt-Rink, 1986). As the plasma density increases, the energy of free e–h pairs becomes renormalized (band gap renormalization), whereas that of the bound states hardly changes because of their charge neutrality. The binding energy of the bound states measured from the renormalized continuum decreases. The resonances lose oscillator strength, both because of the occupation of states out of which excitons are constructed (phase space filling) and because of the loss of e–h correlation (i.e. the excitons are becoming larger). The width of the peaks increases because of collisional

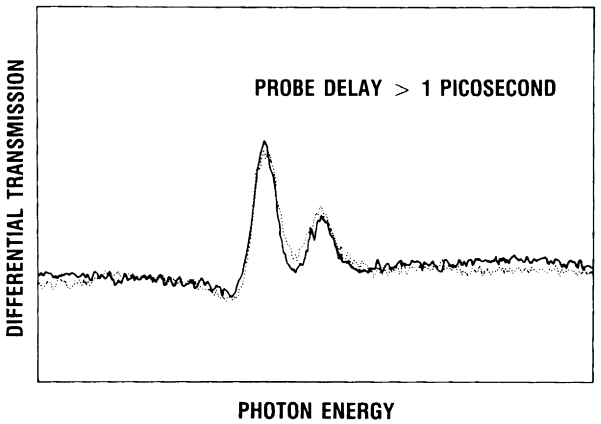

Figure 3. Differential transmission spectra for selective generation of hh-excitons (full line) and free e–h pairs (dotted line), after exciton ionization and thermalization of the e–h plasma.

broadening. At low densities, when the continuum is still far from the resonances, only the loss of oscillator strength and the broadening are apparent. However, if the density continues to increase, the resonances merge in the continuum, and eventually this continuum edge is the only remaining spectral feature. It is remarkable that in the case of high-quality GaAs–AlGaAs QWs, the profile of the final edge is exactly that of the broadened 2D continuum used to fit the unperturbed spectrum. This is shown in Fig. 4. The dots are obtained from the first ($N \sim 0$) and last ($N \sim 2 \times 10^{12}$ cm^{-2}) digitized spectra of Fig. 2, and the full lines correspond to the semi-empirical fit just described. In the upper part of the figure, the broadened continuum is also shown. A rigid red shift of ~ 17 meV of this continuum suffices to give an almost perfect coincidence with the high-density spectrum as shown in the lower part of the figure.

An interpretation similar to that given in the previous paragraph explains the saturation measurements performed under cw resonant pumping shown in Fig. 5 (Miller et al., 1982b). The experimental points (open circles) are very well fitted by the sum of two Lorentzian saturation expressions (full line). One corresponds to a species with very low saturation intensity ($I_s \sim 0.58$ kW cm^{-2}) and accounts for the hh-exciton bleaching. The other species is much harder to saturate ($I_s \sim 4.4$ kW cm^{-2}); it corresponds to the bleaching of the band-to-band transitions when the renormalized edge has shifted below the former position of the hh-exciton.

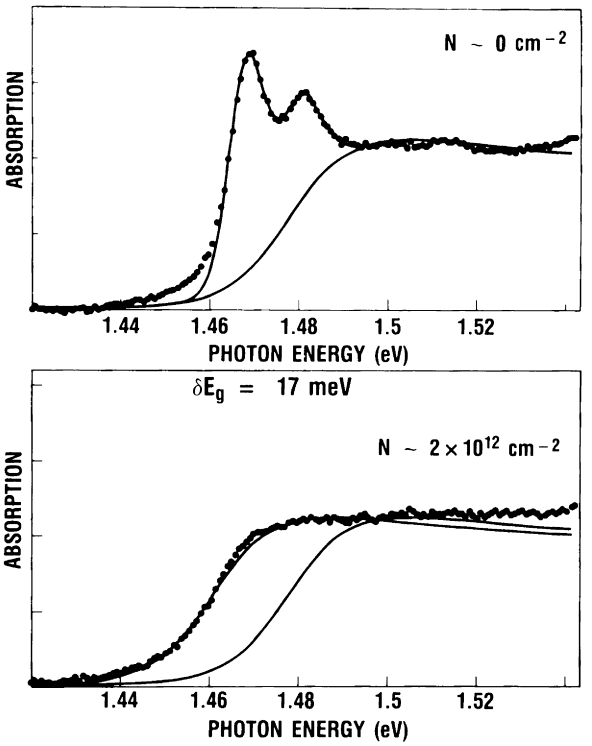

Figure 4. Semi-empirical fits of absorption before (upper part) and after (lower part) excitation. The first fit comprises two Gaussian resonances and a broadened continuum (also shown). The second uses only the 2D continuum rigidly shifted by $\delta E_g \sim 17$ meV.

Additional information on the refractive index effects were obtained from degenerate four-wave mixing (DFWM) experiments using tunable ps pump and probe lasers (Miller et al., 1983a; Chemla et al., 1984). In the low-density region, the bleaching of the exciton can be characterized by a nonlinear absorption cross section σ and a nonlinear refractive index η, which measure, respectively, the change of the absorption coefficient and refractive index induced by one e–h pair

$$\alpha = \alpha_0 - \sigma \bar{N} \tag{7a}$$

$$n = n_0 - \eta \bar{N} \tag{7b}$$

In these equations, in order to be consistent with the usual definitions, $\bar{N}$ is the pair density per unit volume. σ and η are related by the Kramers–Kronig

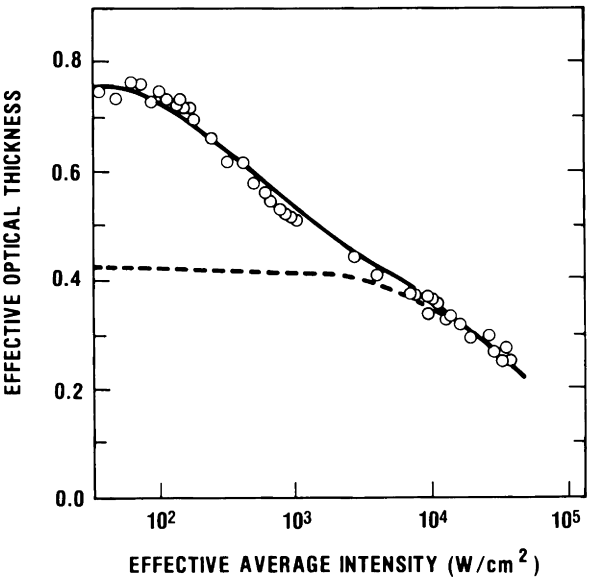

Figure 5. Saturation of the hh-exciton resonance measured under cw excitation (open circles). The full line corresponds to two Lorentzian saturable absorbers. One is very easy to saturate and corresponds to the hh-exciton bleaching. The other is much harder to saturate and corresponds to the bleaching of the renormalized continuum.

relations; together they determine the DFWM diffraction efficiency. Fig. 7 shows the spectra of σ and η, as obtained from a semi-empirical fit of the measured change in transmission shown in Fig. 6. The nonlinearities are extremely large and peak at $\sigma \sim 7 \times 10^{-14}$ cm^2 and $\eta \sim 3.7 \times 10^{-19}$ cm^3. Fig. 6c shows a comparison of the measured diffraction efficiency with the theoretical prediction based on the spectra of σ and η. The agreement is excellent.

The impressive magnitude of the room temperature nonlinear effects in GaAs–AlGaAs QWs was demonstrated by degenerate four-wave mixing using as the sole light source a cw laser diode. A diffraction efficiency of $\sim 0.5 \times 10^{-4}$ was observed in a 1.25 μm sample, using only a ~ 17 W cm^{-2} pump intensity (Miller et al., 1983b). Optical (bistable) devices using GaAs–AlGaAs and InGaAsP–InP QWs as the active medium in nonlinear Fabry–Perot etalons have been operated and have raised much interest for applications in all-optical logic (Peyghambarian and Gibbs, 1985; Tai et al., 1987a). It is likely however that these devices considerably exceed the densities at which the excitons cease to exist and that they rely on interband

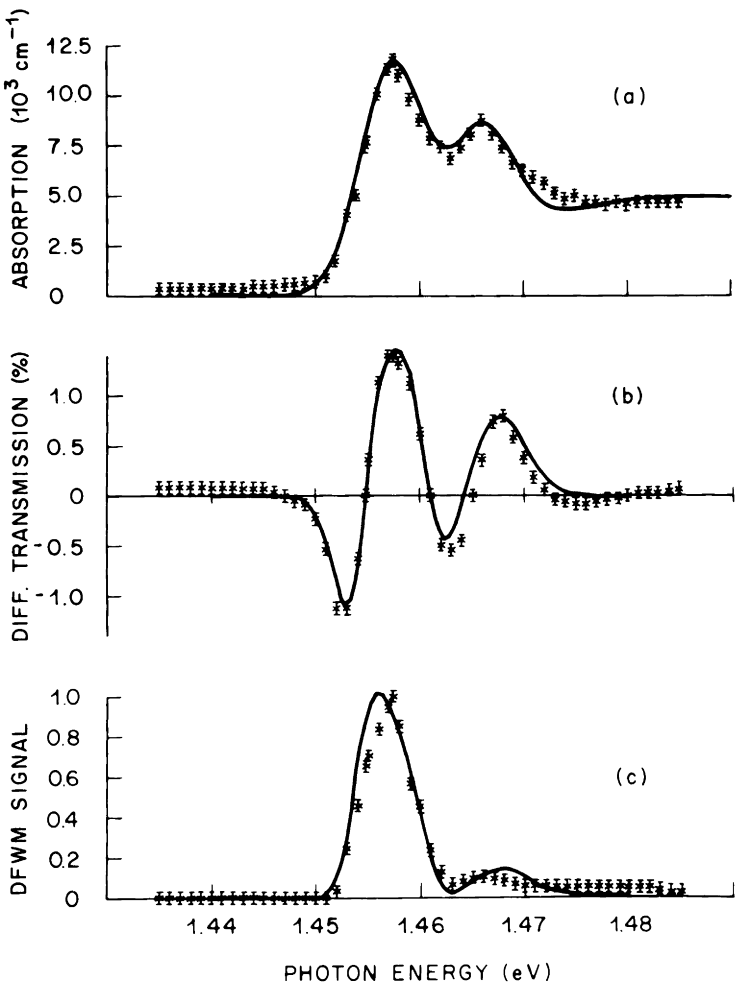

Figure 6. Semi-empirical fits of absorption (a) and differential transmission (b). The theoretical DFWM spectrum, shown by the full line in (c), is obtained from the nonlinear cross sections σ and η shown in Fig. 7.

saturation to complete the switching. GaAs–AlGaAs QWs have been used as saturable absorbers to passively mode-lock GaAs diode lasers. Stable operation producing pulses as short as 1.6 ps has been demonstrated (Smith et al., 1985).

As mentioned in Section III, recently the extreme sensitivity of excitons to the presence of an e–h plasma has been exploited to investigate the very low residual absorption at photon energies well below the band gap in QW

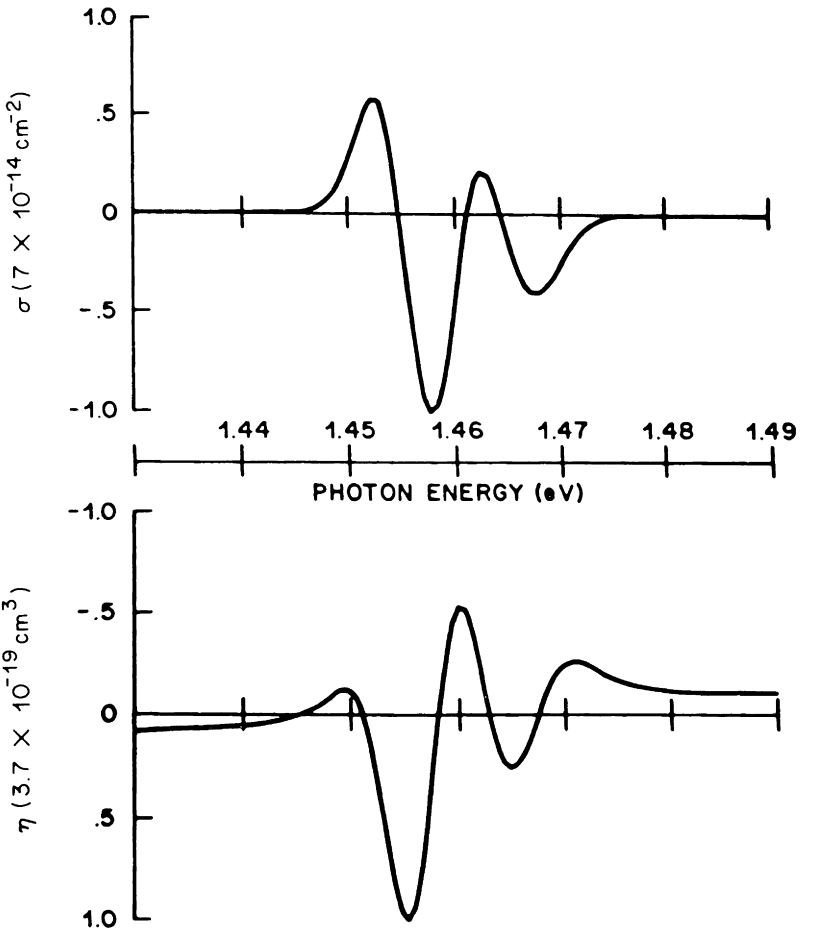

Figure 7. Nonlinear absorption and refraction spectra. σ and η describe respectively the change of absorption and refractive index induced by one e–h pair and are obtained from the fits shown in Fig. 6a and b.

structures. This includes the investigation of the so-called Urbach tail and of phonon side bands, processes in which a photon and some LO phonons are simultaneously absorbed (Liebler et al., 1985). The cross sections for these processes are very small. Until recently, they had been observed only in bulk materials (Sturge, 1962). It is extremely difficult to measure by classical methods such a small absorption in a micron thick QW and new nonlinear optical methods have to be devised to perform these investigations. Since the final result of absorption is the generation of real e–h pairs,

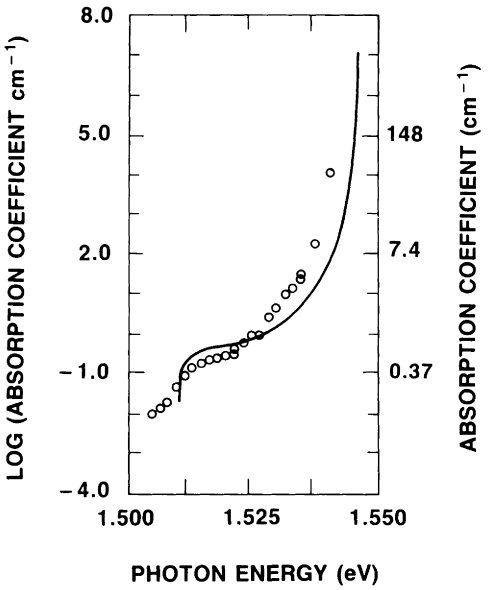

Figure 8. Below-gap LO phonon-assisted absorption. The open circles are measurements using a new nonlinear technique discussed in the text. The full line shows the one-LO-phonon contribution calculated from perturbation theory.

a very weak test beam can be used to probe the transmission of a sample at the peak of the hh-exciton resonance as a very intense pump beam excites the QW structure well below the gap. As the pump frequency is tuned, the test beam measures the directly or indirectly produced e–h plasma density and, hence, in the small signal regime, it maps out the pump absorption (Von Lehmen et al., 1986a, 1987). At high temperatures, when the phonon population is large, the below-gap absorption is found to follow the usual exponential Urbach's rule. However, at low temperatures, a kink appears approximately one LO-phonon energy below the hh-exciton resonance, as clearly shown by the experimental data (open circles) in Fig. 8 for a GaAs–AlGaAs QW at 77 K. This spectral feature corresponds to the one-LO-phonon edge; its profile and position are in remarkable agreement with an extension of the 3D second-order perturbation theory (Segall, 1966) to the 2D case, retaining as the final state the 1s state only. The theoretical line shape (full line) calculated without adjustable parameters agrees very well with the data. The agreement can be improved further if the zero-LO-phonon process on the high-energy side and many-phonon processes on the low-energy side are accounted for. Below the one-LO

–phonon edge, the absorption, although nonzero, is extremely small ($\sim 0.1\,\mathrm{cm}^{-1}$).

B. Nonlinear Optical Effects Induced by Excitons and Nonthermalized Plasmas

Exciton populations can be generated selectively by resonant excitation. At low temperatures, the lowest-energy excitons are stable and only disappear by recombination, a rather long process with characteristic times ranging from nanoseconds or hundreds of picoseconds for dipole-allowed recombination to seconds for the forbidden ones. At high temperatures, the excitons are unstable against collisions with energetic phonons and on the average live only for a time of the order of the mean collision time. As we discussed in Section III, in QWs this corresponds to a fraction of a ps; thus, ultrafast fs spectroscopic techniques are necessary to investigate exciton-induced nonlinear optical effects (Peyghambarian et al., 1984; Knox et al., 1985). In these experiments, a very weak broad-band fs continuum is used to probe over a large spectral range the transmission of a sample at tunable delay from a narrow-band fs pump.

In bulk materials, it was found that excitons produce much weaker nonlinear optical effects than plasmas (Fehrenbach et al., 1982). These observations have been interpreted as follows. In 3D, the dominant mechanism governing the bleaching of exciton resonances is the screening of the e–h interaction (i.e. the exciton state can disappear due to a Mott transition before phase space filling becomes strong). The screening by a plasma is extremely effective compared to screening by excitons because of the absence of a gap in the plasma's excitation spectrum. In the static long-wavelength limit, the presence of a plasma transforms the Coulomb potential into a Yukawa potential and the condition for the disappearance of bound states is the famous Mott criterion $\kappa_{3D} a_0 \sim 1$, where κ_{3D} is the inverse 3D screening length. Actually, the plasma cannot respond instantaneously to the sudden appearance of an e–h pair during the absorption process (charge density fluctuations can only develop in times of the order of the inverse plasma frequency) so that the screening is somewhat weaker. Nevertheless, intraband transitions in a plasma are not energy consuming, whereas excitons can only screen by transitions from their ground state to some excited state. Because of the gap in the excitation spectrum, this

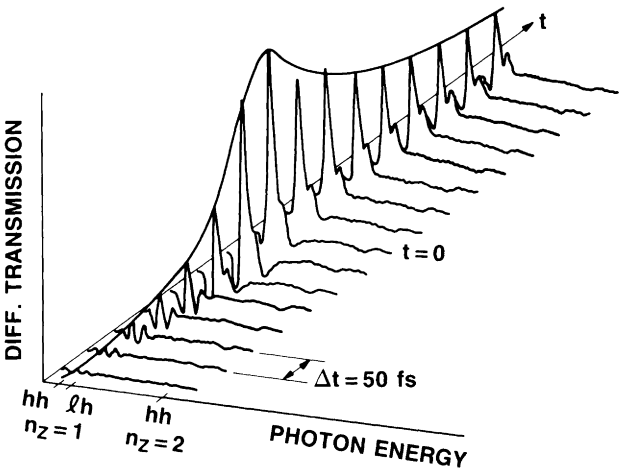

Figure 9. Differential transmission spectra measured with a broad-band 50-fs probe pulse in 50-fs intervals before and after resonant hh-exciton excitation with a 100-fs pump pulse. Initially, the absorption is reduced efficiently as excitons are created in the sample. It then recovers in ~ 300 fs as the excitons are ionized by collisions with thermal LO phonons. The absorption then settles at the same value as it would under cw excitation.

requires some energy so that screening by excitons is much weaker than plasma screening.

According to this picture, resonant exciton creation at room temperature should produce a weak bleaching of the exciton resonances that would increase substantially as the inefficient excitons transform into an efficient plasma. Experiments designed to observe this effect in QWs lead to different and surprising results that we discuss now (Knox et al., 1985). Fig. 9 shows differential transmission spectra measured with a broad-band 50 fs probe pulse in 50 fs intervals before and after resonant hh-excitation by a 100 fs pump pulse. Each spectrum corresponds to the integration of 2×10^6 shots and the resulting signal-to-noise ratio is $\sim 10^4$. The pump intensity is moderate and generates approximately $N \sim 2 \times 10^{10}$ cm^{-2} excitons. Instead of the expected delayed bleaching, one sees during the first half ps a very strong reduction of the absorption at the hh-exciton resonance, which then recovers in about one ps. The spectrum settles at the same level as in the case of thermalized plasma bleaching discussed in Section IV.A. The evolution of the hh-exciton bleaching is well described by the generation of excitons (the total number of excitons generated following the integral of the pump pulse), with subsequent exciton transformation

into free e–h pairs in a 300 fs ionization time. The time constant of the process is in remarkable agreement with that evaluated from the thermal broadening (Section III). However, the surprising result is that the transient population of excitons produces a bleaching about twice as efficient as that of the thermalized plasma. The comparison of the differential spectra lineshape under resonant and above-gap nonresonant pumping (discussed shortly) also indicates that the bleaching mechanism is quite different from screening (Chemla and Miller, 1985). These results force us to reconsider the extension of the picture given above to QWs and room temperature.

The 2D nature of the effects was checked by investigation of single QW waveguides. Indeed, in multiple QW structures, it is possible that carriers generated in different layers interact via long-range Coulomb forces. Measurements of the exciton saturation using ps excitation show that, up to densities at which the exciton peak bleaches significantly, single-QW and multiple-QW structures behave similarly (Weiner et al., 1985b). This suggests that long-range Coulomb forces are effective within the same layer only or that they are not very important with respect to the exciton bleaching, in both single and multiple QWs.

In order to understand these results, one has to reconsider the basic mechanisms that can contribute to the bleaching of the exciton resonance. (We shall give a somewhat simplistic discussion here. See also Schmitt-Rink et al., 1985.) A somewhat deeper discussion of what is going on in 2D has been given elsewhere by one of us (Schmitt-Rink, 1986). In addition to the aforementioned direct screening (S), the absorption strength of exciton resonances can be diminished by the effects of the exclusion principle, phase space filling (PSF) (often referred to as "blocking") and fermion exchange (E); states in phase space that are already occupied are no longer accessible in optical transitions or available for exciton formation. Put in simple terms, one cannot optically create two e–h pairs (bound or free) on top of each other if they require the same $\underline{k}$-states. These effects involve only fermions of the same spin and are, of course, most efficient at short distances, whereas S is a long-range Coulomb effect. In 1D and 2D, particles see "more" of their near neighbors than in 3D, which suggests already at this point that "overlap" and "statistical" effects are more pronounced.

The effects of Pauli exclusion in an e–h plasma are well known. (For example, in the case of band-to-band transitions, PSF leads to the Burstein–Moss shift.) Their description requires the knowledge of the fermion distribution functions $f_e(k)$ and $f_h(k)$. In the case of an e–h plasma and depending on the temperature, $f_{e,h}(k)$ are given by Fermi or

Boltzmann distributions. To extend this principle to an exciton gas, it is only necessary to note that the resonant creation of one 1s exciton (at the bottom of its band) corresponds to an occupation probability $|U_{1s}(k)|^2$ in fermion space, which is equally shared between spin up and down particles, so that

$$f_e(k) = f_h(k) = N|U_{1s}(k)|^2/2 \tag{8}$$

where N in this case is the exciton density. This very intuitive result is, of course, theoretically substantiated (Comte and Nozieres, 1982; Haug and Schmitt-Rink, 1984; Schäfer and Treusch, 1986).

As for the effects of screening in 2D, various arguments can be given that they are much weaker than in 3D. Plasma S is determined by the number of carriers that can undergo intraband transitions and thus is proportional to the density of states (DOS). In 2D, the DOS is constant and hence the screening is weaker than in 3D. In particular, in the degenerate limit, the 2D Thomas–Fermi screening length reduces to a constant (Ando et al., 1982). This leads an extension of the 3D Mott criterion to 2D ad absurdum and shows that it is also rather meaningless to extend the random phase approximation (RPA) to 2D. All results will depend on the behavior of the screening at short distances, the proper description of which is outside the range of mean field theories. Much the same can be said for the nondegenerate limit, in which the breakdown of the RPA is signaled by the logarithmic divergence of the Debye shift (Totsuji, 1975; Haug and Schmitt-Rink, 1985; Schmitt-Rink, 1986). Obviously, what has to be accounted for is the exchange-correlation hole surrounding each particle (Schmitt-Rink, 1986). Particles of identical spin or charge try to avoid each other, which hinders the piling up of a screening charge. This reduces the screening beyond its mean field value. One further phenomenon worth mentioning is the important fact that in 1D and 2D, an arbitrarily small attractive potential always supports at least one bound state (similarly, all states are localized in 1D and 2D disordered systems). Plasma screening is strongest in the static long-wavelength limit, but even in that limit, it cannot ionize an exciton, in contrast to 3D systems.

The consequences of these characteristic properties of 2D systems for excitonic nonlinear optical effects were not considered until recently (Schmitt-Rink et al., 1985; Schmitt-Rink, 1986). If the effects of S are weak in QWs, then the bleaching of the exciton resonances by PSF and E will be related to the overlap of the electron and hole distributions in a plasma or in a resonantly excited exciton gas with the portion of the Brillouin zone that participates in the exciton wave function. Thus, a cold plasma, for

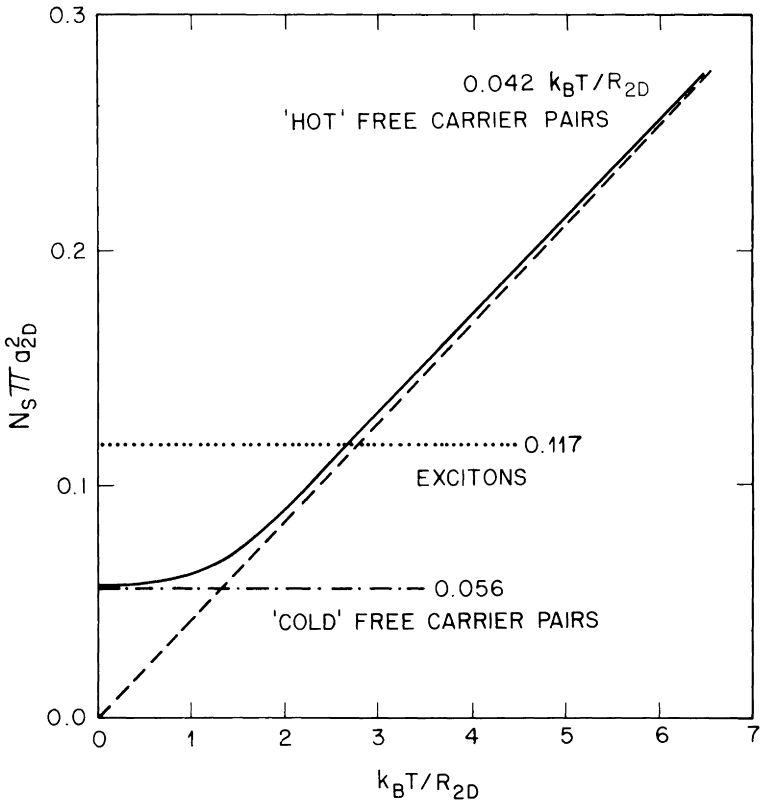

Figure 10. Comparison of the effects of Pauli exclusion (phase space filling and fermion exchange) induced by an exciton gas (dotted line), a "hot" e–h plasma (dashed line), and a "cold" e–h plasma (dashed-dotted line). The full line is a sketch of the transition from one limit to the other and is not calculated.

which $f_{e,h}(k)$ are Fermi distributions located at the bottom of the bands, should bleach more efficiently than the "zero temperature" exciton gas, for which $f_{e,h}(k)$ are given by Eq. 8. In turn, the exciton gas will be more efficient than a hot plasma as soon as the thermal spread of the Boltzmann distributions in k-space exceeds the inverse exciton Bohr radius. The correct theoretical description of PSF and E effects indeed confirms this intuitive analysis as shown in Fig. 10, where the respective 2D saturation densities N_s are plotted. This accounts then for the experimental observations, which are nothing but a comparison on a fs time scale of the effects of a resonantly excited exciton gas at short times to those of a hot (room temperature) e–h plasma at long times, the former effect being larger than the latter.

The theoretical results for the effects of PSF and E on 2D excitons shown in Fig. 10 have been obtained from an approximate calculation of the 1s exciton orbital wave function U_{1s}, as modified by the presence of other e–h pairs (Schmitt-Rink et al., 1985). The difference due to Pauli exclusion between the perturbed and unperturbed e–h relative motion Hamiltonians in momentum space is

$$\langle \underline{k}|\delta H|\underline{k}'\rangle_E = -\delta_{\underline{k},\underline{k}'}\sum_{\underline{k}''} V(\underline{k}-\underline{k}'')\left[f_e(k'')+f_h(k'')\right] + V(\underline{k}-\underline{k}')\left[f_e(k)+f_h(k)\right] \tag{9}$$

where $V(q)$ is the bare Coulomb interaction. The first term in Eq. 9 is a self-energy correction that comprises the electron and hole exchange self-energies, i.e. the energies that parallel spin particles gain by avoiding each other. The second term is the corresponding vertex correction, which describes the weakening of the attractive e–h interaction due to the exclusion principle. Screening would give rise to further corrections, except that for 2D systems we do not quite know how to treat it rigorously. In any case, as just discussed, we expect Eq. 9 to contain the major physics and the corrections due to screening to be relatively unimportant for the present discussion.

According to Eq. 4, the 1s exciton oscillator strength f_{1s} is proportional to the probability $|U_{1s}(r=0)|^2$ to find the e and h in the same unit cell. Through the first-order modification of U_{1s}, the perturbation Eq. 9 gives rise to a relative change in oscillator strength

$$\left.\frac{\delta f_{1s}}{f_{1s}}\right|_E = \sum_{n\neq 1s}\left[\frac{\langle n|\delta H|1s\rangle_E}{E_{1s}-E_n}\frac{U_n(r=0)}{U_{1s}(r=0)} + \frac{\langle 1s|\delta H|n\rangle_E}{E_{1s}-E_n}\frac{U_n^*(r=0)}{U_{1s}^*(r=0)}\right] \tag{10}$$

Consistent with Eq. 10, the change due to the blocking of the final 1s state is

$$\left.\frac{\delta f_{1s}}{f_{1s}}\right|_{PSF} = -\sum_{\underline{k}}\left[f_e(k)+f_h(k)\right]\frac{U_{1s}(k)}{U_{1s}(r=0)} \tag{11}$$

Both changes are, of course, fundamentally related; Eq. 11 is nothing but the correction to f_{1s} due to the proper normalization of U_{1s} in the presence of other pairs. Remembering that $U_{1s}(r=0) = \Sigma_{\underline{k}} U_{1s}(k)$, Eq. 11 can be simply interpreted as the average occupation of the components of the wave function in $\underline{k}$-space.

In leading order in the e–h pair density N, the relative change of the optical susceptibility χ in the spectral vicinity of the 1s exciton resonance

can be written as

$$\frac{\delta\chi}{\chi} = -\frac{N}{N_s} = -N\left[\frac{1}{N_s^{E}} + \frac{1}{N_s^{PSF}}\right] = \lim_{N\to 0}\left[\left.\frac{\delta f_{1s}}{f_{1s}}\right|_{E} + \left.\frac{\delta f_{1s}}{f_{1s}}\right|_{PSF}\right] \tag{12}$$

where N_s is the overall saturation density and N_s^{E} and N_s^{PSF} are the saturation densities associated with exchange and phase-space filling respectively. This accounts automatically for the saturation behavior observed under cw pumping (Section IV.A). To evaluate Eq. 12, we need to perform the summation over all excited exciton states in Eq. 10. When the summation is carried out over the complete set of uncorrelated pair (plane wave) states, the following analytical results are obtained:

$$N_s \pi a_{2D}^2 \sim 0.117 \tag{13}$$

for the selective generation of 2D excitons and

$$N_s \pi a_{2D}^2 \sim 0.056, \qquad k_B T \ll R_{2D} \tag{14a}$$

$$\sim 0.042 \frac{k_B T}{R_{2D}}, \qquad k_B T \gg R_{2D} \tag{14b}$$

for the generation of a thermalized 2D e–h plasma. These results have the following intuitive interpretation. When an exciton is created, the area occupied by it cannot sustain more excitons (Eq. 13). If we assign to the exciton some effective "hard disk" radius of the order a_{2D}, two disks of this radius cannot share the same space. Much the same can be said for cold free carriers (Eq. 14a). A single carrier cannot occupy the space occupied by an exciton and vice versa. Even in the case of hot free carriers (Eq. 14b), the same notion can be retained, only now we must note that only a fraction of the order $(\lambda/a_{2D})^2 \sim R_{2D}/k_B T$ occupy the phase space sampled by an exciton (λ is the thermal wavelength); i.e. a carrier with thermal energy greater than the exciton binding energy can occupy the same space as an exciton without violating Pauli exclusion.

Equations 13 and 14b explain all experimental results quantitatively (within a factor of 2), without any adjustable parameters, which is quite remarkable in view of the various approximations made.

The simple theory outlined in the previous paragraphs assumed that in 2D, screening is weak as compared to the effects of the Pauli principle. In order to test this hypothesis, a direct experimental comparison of PSF and E with S has been performed (Knox et al., 1986). The principle of these

investigations is the following. Using fs laser pulses, it is possible to generate nonthermal carrier distributions in the continuum between the $n_z = 1$ and 2 resonances and to observe their effects on the absorption spectrum before and during their relaxation to the bottom of the band. If the excess energy is less than one LO phonon energy, exchange of energy with the lattice will take a rather long time and the carriers will first thermalize among themselves before reaching an equilibrium with the lattice. Immediately after excitation, the carriers do not occupy states out of which the $n_z = 1$ and 2 excitons are constructed and, thus, the PSF and E are not effective, whereas screening is right away effective. As the carriers equilibrate among themselves, their distribution evolves toward a thermal one and they start to fill up states at the bottom of the $n_z = 1$ subbands. Therefore, they produce PSF and E on the corresponding excitons. Only the high-energy tail of the thermalized distribution will extend up to the bottom of the $n_z = 2$ subbands, which in any case are almost orthogonal to the $n_z = 1$ subbands, so that for these resonances, PSF and E remain ineffective. Therefore, the evolution of the absorption at the $n_z = 1$ excitons during thermalization will first show the effects of S and then how the PSF and E are turned on, whereas at the $n_z = 2$ resonance there should be only little (if any) change during thermalization. Then, on a much longer time scale, the carriers will equilibrate with the lattice and eventually recombine.

This process is shown in Fig. 11, where differential transmission spectra in 50 fs intervals from 100 fs before to 200 fs after arrival of a 100 fs pump pulse are presented. The spectral distribution of the pump photons is shown at the bottom of the figure, the pump pulse produces approximately $N \sim 2 \times 10^{10}\,\mathrm{cm}^{-2}$ e–h pairs. Immediately upon arrival of the pump pulse, one sees absorption changes at the $n_z = 1$ and 2 resonances as well as a spectral hole burning in the continuum, corresponding to state filling by the nonthermal carrier distributions. The $n_z = 1$ excitons lose some oscillator strength and broaden slightly, whereas the $n_z = 2$ exciton experiences also a slight red shift. These changes are consistent with those due to the S of a plasma discussed in Section IV.A. Note that such small effects can only be seen because of the enormous improvements of fs spectroscopic techniques (Fork et al., 1981; Knox et al., 1984). As the carriers start to thermalize, the spectral hole in the continuum changes shape and shifts to lower energies. Accompanying this thermalization, the bleaching of the $n_z = 1$ resonances increases and finally settles after 200 fs at the same level as in the case of thermalized plasma generation discussed previously. The changes at the $n_z = 2$ resonance remain essentially the same, showing that the S has not changed significantly. Comparison of the $n_z = 1$ bleaching at $t = 0$ and

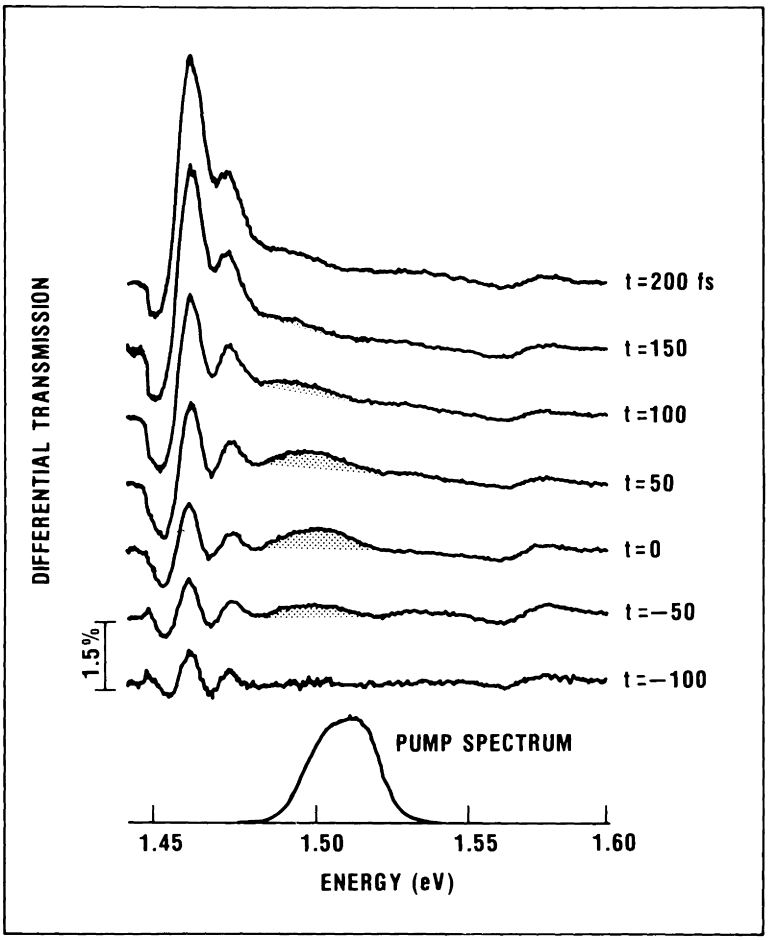

Figure 11. Differential transmission spectra measured with a broad-band 50-fs probe pulse in 50-fs intervals before and after excitation of nonthermal e and h distributions by a 100-fs pump pulse. Initially, the pump burns a spectral hole in the absorption spectrum, which then thermalizes within ~ 200 fs. During thermalization, the effects of the Pauli principle at the $n_z = 1$ resonances are "turned on."

after $t = 200$ fs shows that the combined effects of PSF and E are at least six times larger than those of S (the measurements can only give a lower bound for the ratio [PSF + E]/S, because it is always possible for some carriers to be generated by the very front edge of the pulse and thus to thermalize early). These experiments confirm that the effects of plasma S on excitons are strongly reduced in 2D as compared to 3D. They also contain a

wealth of information about carrier relaxation in these important microstructures that is not directly relevant to our present discussion.

Yet another, although more indirect, confirmation of the theory was obtained from the study of the exciton shift in QWs at low temperatures (Peyghambarian et al., 1984; Hulin et al., 1986a; Masumoto et al., 1986). In 3D, the exciton resonances hardly change their position as the density of excitons increases. This can be explained by an almost perfect cancellation of the blue shift due to Pauli exclusion (short-range hard core repulsion) (Comte and Noziéres, 1982) and the red shift due to screening (long-range Van der Waals attraction) (Noziéres and Comte, 1982). In 2D QWs, the blue shift due to Pauli exclusion is no longer balanced and thus should be measurable (Schmitt-Rink et al., 1985; Schmitt-Rink, 1986). At low temperatures, the Hartree contribution to the shift of the exciton (expectation value of Eq. 9 in the 1s state) is given by (Schmitt-Rink et al., 1985; Bobrysheva et al., 1980)

$$\delta E_{1s}^{2D} = 16\pi N a_{2D}^2 (1 - 315\pi^2/2^{12}) E_{1s}^{2D} \tag{15}$$

Experiments performed on QWs of various thicknesses have shown this blue shift when excitons are selectively generated or when they are formed after a few ps from nonresonantly excited e and h. The shift is rather difficult to observe in thick layers but is very pronounced in the narrowest QW, where the dimensionality approaches the pure 2D limit. Its magnitude has been found to be in surprisingly good agreement with the theory (Hulin et al., 1986a). A blue shift was also observed in layered semiconductors, such as BiI_3 (Watanabe et al., 1986).

C. Field-induced Nonlinear Optical Effects

Coherent nonlinear optical processes are produced by the excitation of semiconductors in the transparency region well below the absorption edge. These effects are often referred to as "nonresonant" (Bloembergen, 1965), in the sense that the excitation does not coincide with an absorption resonance; they do have resonant enhancements as such absorption resonances are approached. Such nonlinearities have been widely investigated in the near and medium infrared (Chemla, 1980). The physical mechanisms that produce them can be described as follows. The valence electrons are held in equilibrium by the large atomic fields, which are of the order of $E_{at} = 10^8$–10^9 V/cm; the application of optical fields $E(\omega)$ not negligible as compared to E_{at} induces anharmonic charge density flucations that in turn can interact with other optical fields $E(\omega')$. The mutual coupling of the

$E(\omega)$ and $E(\omega')$ via the anharmonic charge density fluctuations causes exchange of photons among the optical fields. In the process, however, no energy is deposited in the material. The nonresonant effects are characterized by the fact that below-gap optical fields induce only virtual populations, which last as long as the fields are applied.

In the (textbook) quantum mechanical description of these processes, the "ground state" of the semiconductor in the presence of the optical fields is represented by a coherent superposition of excited (e–h) states. The expectation value of the polarization is calculated (at least formally) using the density matrix formalism. In most cases, spatial dispersion is negligible and only dipolar effects are retained. They are described by an interaction Hamiltonian of the form $-P \cdot E$, where P is the polarization of the medium. In the classical discussion of nonlinear optics, the expectation value of P is expanded in a power series of the $E(\omega)$'s, the coefficients being the nonresonant nonlinear susceptibilities $\chi^{(3)}$, $\chi^{(5)}, \ldots$. Finally, the field interaction is analyzed by solving the corresponding Maxwell equations coupled by the nonlinear polarizations (Shen, 1984).

The formal expressions of the nonlinear susceptibilities are written in terms of excited state wave functions and energies, which are usually not known. Most of the time they are treated as phenomenological parameters that are determined experimentally. Specific experimental investigations of excitonic effects in nonresonant nonlinear optical processes have been rather scarce and theoretical models have been limited to semi-empirical descriptions, where the exciton levels are characterized by ad hoc matrix elements and spectroscopically determined energies.

It is obvious that e–h, e–e and h–h correlation effects must play a crucial role in nonresonant nonlinear optical processes because of the strong coupling induced between the charge density fluctuations by the Coulomb forces. It is also clear that the effects of the Coulomb correlation must be treated in a self-consistent manner with the effects of the applied fields. Therefore, the correct description of nonresonant excitonic nonlinearities in semiconductors cannot follow a simple transposition of the description of atomic nonlinear optical processes. In this section, we review recent experimental investigations of these effects in GaAs QWs (Mysyrowicz et al., 1986; Von Lehmen et al., 1986b) and a theory that, for the first time, correctly accounts for exciton correlation effects on "nonresonant" nonlinear susceptibilities (Schmitt-Rink and Chemla, 1986).

How can excitonic effects be resolved in below-gap nonlinear optical processes? Obviously, they influence the absolute magnitude of the susceptibilities $\chi^{(n)}$. In practice, however, the determination of these quantities is

not very useful because (1) they are rather difficult to measure accurately and (2) the $\chi^{(n)}$ are global parameters involving infinite sums over complete sets of states, in which the behavior of particular states is difficult to isolate. It is thus more interesting to turn to spectroscopic measurements.

Clearly, the most natural way to probe excitonic effects is to probe the absorption spectrum while the sample is strongly excited well below the gap and to look for transient changes that persist only as long as the excitation. It is fair to say that these effects were first observed accidentally. In time-resolved studies of the below-gap absorption in QWs (Section IV.A), strong and transient changes of the probe transmission, as shown in Fig. 12, were observed (Von Lehmen et al., 1986b). These changes can be positive or negative depending on the position of the test photon energy with respect to the peak of the hh-exciton. They last only as long as the pump pulse. If the detuning from the exciton resonance is not too large, as in Fig. 12, much weaker effects due to a photo-generated plasma are also seen. This process is easily distinguished from the field effects. It persists for the lifetime and completely disappears for large detuning. The fast component of the change in probe absorption was studied as a function of the pump parameters. It was found that it is linear in the inverse pump detuning $(E_{1s} - \hbar\omega_p)^{-1}$ for a fixed pump intensity (Fig. 13a), and linear in the pump intensity for a fixed pump detuning (Fig. 13b). Furthermore, a lineshape analysis of the fast and slow components as a function of the probe frequency around the $n_z = 1$ resonances evidences their very different spectral profiles (Von Lehmen et al., 1986b). The slow component has all the characteristics of the plasma-induced bleaching and broadening discussed in Section IV.A. The fast component is much larger and its differential transmission spectrum corresponds to a transient blue shift of the exciton resonances. For a pump detuning $\sim$ 30 meV and a pump intensity $\sim$ 8 MW/cm^2 the magnitude of the shift is $\sim$ 0.2 meV for the hh-exciton peak and $\sim$ 0.05 meV for the lh-exciton peak. The same effects have also been observed using fs pump and continuum probe pulses, although at much higher pump intensity (Mysyrowicz et al., 1986). Again, they were found accidentally in the study of the blue shift induced by real exciton populations (Section IV.B). In addition, in these experiments there is clear evidence of a loss of excitonic oscillator strength. In conclusion, the main effects of the strong below-gap excitation on the transmission of a weak test beam are a shift and bleaching of the resonances, henceforth referred to as the AC Stark effect.

How does this semiconductor AC Stark effect relate to the one studied extensively in atomic systems (Mollow, 1969, 1972)? Clearly, in the absence of Coulomb interactions (and thus of excitons), it would not be very

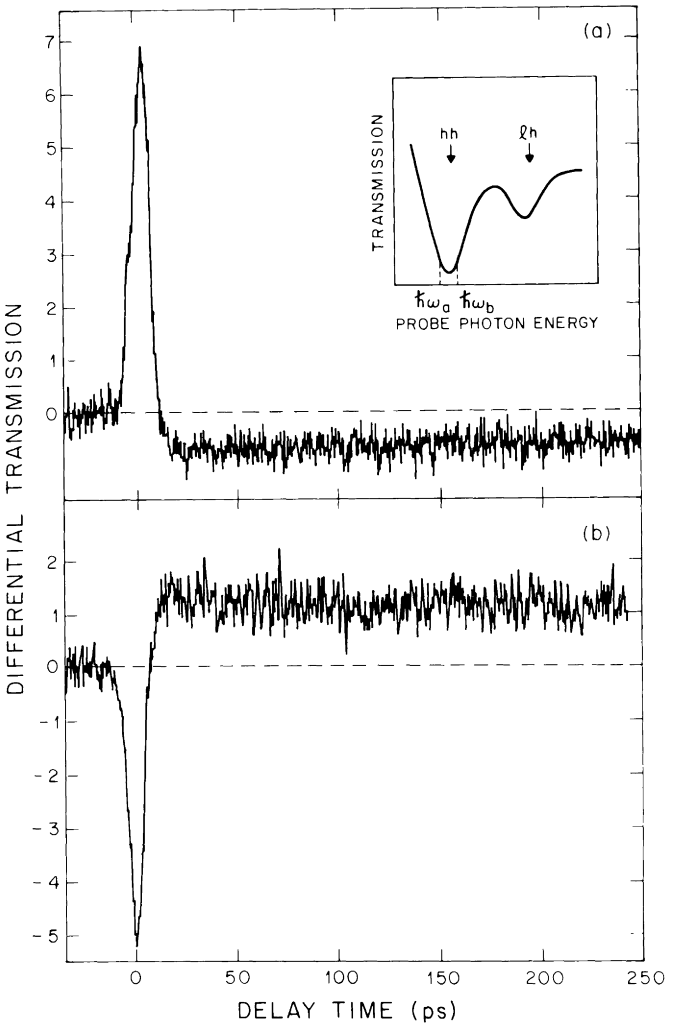

Figure 12. Differential transmission as a function of the pump-probe delay. The pump is tuned ~ 25 meV below the hh-exciton resonance. The probe is tuned ~ 1 meV below the hh-exciton resonance in (a) and ~ 1 meV above the hh-exciton resonance in (b).

different. Interband transitions with different e–h relative momenta $\underline{k}$ would then decouple, and each individual transition would behave in much the same fashion as a two-level atom coherently driven below resonance. The band-to-band transitions would be bleached and blue shifted and, at high pump intensities, optical gain would develop below $2\hbar\omega_p - E_g$. (In the latter process, two pump photons are destroyed and a test photon and free e–h pair are created.) In second order in the pump field E_p, the change in

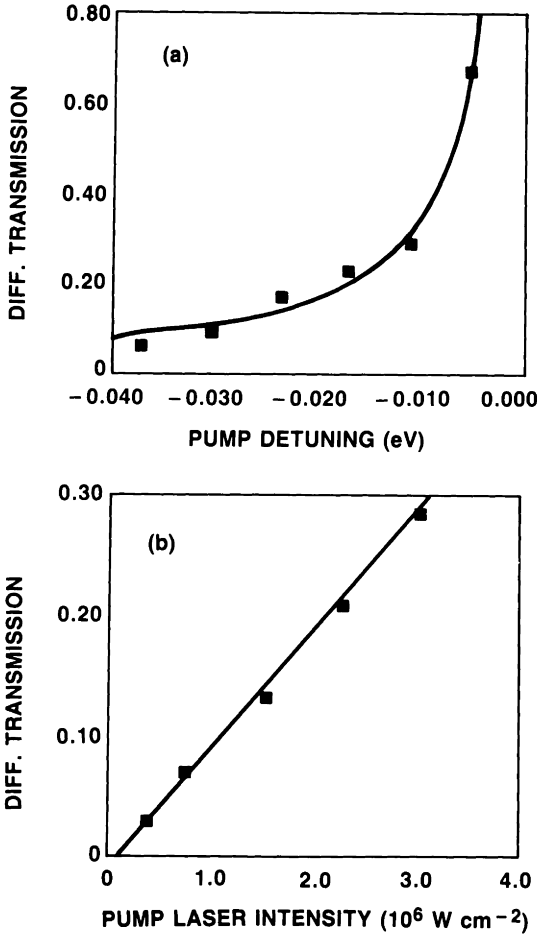

Figure 13. Differential transmission as a function of the pump detuning from the hh-exciton resonance (a) and pump intensity for a fixed pump detuning ~ 18 meV (b).

band gap would be

$$\delta E_g = 2\frac{|er_{cv}E_p|^2}{E_g - \hbar\omega_p} \tag{16}$$

Unperturbed exciton states are a superposition of free e and h states, the coefficients being the relative motion orbital wave functions $U_n(\underline{k})$, subject to

$$\left(E_n - E_g - \frac{\hbar^2 k^2}{2m}\right)U_n(\underline{k}) + \sum_{\underline{k}'} V(\underline{k} - \underline{k}')U_n(\underline{k}') = 0 \tag{17}$$

This simple Schroedinger equation serves to demonstrate how this free e–h picture has to be modified to account for the e–h interaction. Inside an exciton, e–h pair states (and thus interband transitions) with different relative momenta $\underline{k}$ are strongly Coulomb-correlated, so that a pair with given $\underline{k}$ does not only experience the external field $E_{\text{ext}} \equiv E_p$ but also a significant internal one, the "molecular field" E_{mol} associated with virtual pairs created at $\underline{k}'$. Much the same can be said for the effects of the e–e and h–h interaction (see Eq. 9). At each $\underline{k}$, external and Coulomb fields combine to give an effective self-consistent "local field," $E_{\text{loc}} = E_{\text{ext}} + E_{\text{mol}}$ (Schmitt-Rink and Chemla, 1986). The problem is thus similar to that of a paramagnet in an external magnetic field.

For very small external fields, the "molecular fields" or "local field corrections" are large. They transform the free e–h pairs into excitons. (In a paramagnet, this corresponds to the transition from itinerant to local moment behavior.) As the pump field strength increases, so does the number of coherently excited excitons. The virtual exciton states start to interact, in much the same way as if they were actually populated. In fact, we recover Eqs. 9 through 11 if we identify $f_{\text{e, h}}(k)$ with virtual e and h distributions. Considering the leading 1s state contribution only, we can recover Eqs. 8 and 15, where N is now the number of virtually excited 1s excitons

$$N = 2\frac{|er_{cv}E_p|^2}{\left(E_{1s} - \hbar\omega_p\right)^2}|U_{1s}(r=0)|^2 \tag{18}$$

Thus, for not-too-large pump intensities, we can carry over our previous results. The interaction of virtually excited excitons is exactly the same as that of real ones (Schmitt-Rink and Chemla, 1986).

The coherent "ground state" of a semiconductor in the presence of a pump beam is, of course, not what is being measured by a test beam. A weak test beam E_t induces a polarization, which has to be clearly distinguished from that induced by the pump beam. It measures the "excitation spectrum" (Schmitt-Rink and Chemla, 1986).

The Coulomb fields induced by the external perturbation E_t combine to give an effective field $\delta E_{\text{ext}} = E_t + \delta E_{\text{mol}} + \delta E_s$ at each $\underline{k}$. The first two terms ($E_t + \delta E_{\text{mol}}$) account again for the fact that the system responds to the exact local field, the third term describes the screening of the perturbation due to the induced charge density fluctuations. For not-too-large pump intensities, i.e. in the excitonic limit, the evaluation of the excitation spectrum, which determines the linear response to δE_{ext}, is very tedious.

Some of the results, such as the occurrence of excitonic gain below $\hbar\omega_p$, can be guessed. Of special interest here is the AC Stark shift of the exciton resonance. Keeping only the virtual 1s state contribution and neglecting virtual exciton–exciton interactions (which can produce an additional shift), one finds in leading order in the pump intensity (Schmitt-Rink and Chemla, 1986)

$$\delta E_{1s} = 2\frac{|er_{cv}E_p|^2}{E_{1s} - \hbar\omega_p}\frac{|U_{1s}(r=0)|^2}{N_s^{PSF}} \tag{19}$$

where N_s^{PSF} is the saturation density due to excitonic phase space filling, defined in Section IV.B.

First of all, Eq. 19 explains the experimental results, without any adjustable parameters. For the experimental parameters given above, the theoretical hh-exciton blue shift is 0.15 meV and the ratio of the hh-exciton and lh-exciton shifts is 4. The agreement is excellent.

If we identify Eq. 19 with the AC Stark shift in a two-level system, we find that 1 exciton behaves like N_s^{PSF} two-level atoms, a result that we could have also obtained from the discussion given in Section IV.B. Vice versa, the first factor in Eq. 19 expresses the AC Stark shift of the atomic s and p states that form the conduction and valence bands. The second factor describes the renormalization of this atomic shift due to excitonic effects. Its numerator reflects the fact than an exciton is built up from a linear combination of Bloch states that themselves originate from the atomic states. The denominator contains the saturation density N_s^{PSF}, above which the concept of excitons becomes invalid.

Very recently, the AC Stark effect has also been observed in InGaAs–InP QWs (Tai et al., 1987b) and has been exploited to operate a GaAs–AlGaAs optical gate with subpicosecond switch on and off times (Hulin et al., 1986b).

V. CONCLUSIONS

In its few years of existence, the nonlinear optics of quantum wells has already proved to be a fertile ground for novel physics. It has, for example, increased our understanding of the linear optical properties of quantum wells, helping to explain the remarkable persistence of exciton resonances at room temperature. It has enhanced our knowledge of many-body effects in two and three dimensions. It has enabled us to measure the dynamics of particle interactions in confined systems. It has elucidated the many-body

interactions of virtual populations. More generally, however, it has contributed to a growing awareness of the possibilities for new nonlinear optical processes for physics and devices through quantum engineering of small structures. This broader field is only just starting to grow, and it promises to be an exciting one in the years ahead.

REFERENCES

Ando, T., Fowler, A. B., and Stern, F. (1982). *Rev. Mod. Phys.* **54,** 437–672.

Bastard, G. (1984). *Phys. Rev. B* **30,** 3547–3549.

Bastard, G., Mendez, E. E., Chang, L. L., and Esaki, L. (1982). *Phys. Rev. B* **26,** 1974–1979.

Bloembergen, N. (1965). *Nonlinear Optics*. W. A. Benjamin, New York.

Bobrysheva, A. I., Zyukov, V. T., and Beryl, S. I. (1980). *Phys. Status Solidi B* **101,** 69–76.

Broido, D. A., and Sham, L. J. (1986). *Phys. Rev. B* **34,** 3917–3923.

Chang, Y. C., and Schulman, J. N. (1983). *Appl. Phys. Lett.* **43,** 536–538.

Chemla, D. S. (1980). *Rep. Prog. Phys.* **43,** 1191–1262.

Chemla, D. S. (1983). *Helv. Phys. Acta* **56,** 607–637.

Chemla, D. S. (1985). *J. Lumin.* **30,** 502–519.

Chemla, D. S., and Miller, D. A. B. (1985). *J. Opt. Soc. Am. B* **2,** 1155–1173.

Chemla, D. S., and Pinczuk, A., eds.(1986). *IEEE J. Quantum Electron.* **QE-22,** 1609–1921.

Chemla, D. S., Miller, D. A. B., Smith, P. W., Gossard, A. C., and Wiegmann, W. (1984). *IEEE J. Quantum Electron.* **QE-20,** 265–275.

Comte, C., and Nozieres, P. (1982). *J. Physique* **43,** 1069–1081.

Dingle, R., Wiegmann, W., and Henry, C. H. (1974). *Phys. Rev. Lett.* **33,** 827–830.

Elliot, R. J. (1957). *Phys. Rev.* **108,** 1384–1389.

Fehrenbach, G. W., Schaefer, W., Treusch, J., and Ulbrich, R. G. (1982). *Phys. Rev. Lett.* **49,** 1281–1284.

Fork, R. L., Greene, B. I., and Shank, C. V. (1981). *Appl. Phys. Lett.* **38,** 671–672.

Greene, R. L., Bajaj, K. K., and Phelps, D. E. (1984). *Phys. Rev. B* **29,** 1807–1812.

Haug, H., and Schmitt-Rink, S. (1984). *Prog. Quantum Electron.* **9,** 3–100.

Haug, H., and Schmitt-Rink, S. (1985). *J. Opt. Soc. Am. B* **2,** 1135–1142.

Hegarty, J., and Sturge, M. D. (1985). *J. Opt. Soc. Am. B* **2,** 1143–1154.

Hulin, D., Mysyrowicz, A., Antonetti, A., Migus, A., Masselink, W. T., Morkoc, H., Gibbs, H. M., and Peyghambarian, N. (1986a). *Phys. Rev. B* **33,** 4389–4391.

Hulin, D., Mysyrowicz, A., Antonetti, A., Migus, A., Masselink, W. T., Morkoc, H., Gibbs, H. M., and Peyghambarian, N. (1986b). *Appl. Phys. Lett.* **49,** 749–751.

Knox, W. H., Downer, M. C., Fork, R. L., and Shank, C. V. (1984). *Opt. Lett.* **9,** 552–554.

Knox, W. H., Fork, R. L., Downer, M. C., Miller, D. A. B., Chemla, D. S., Shank, C. V., Gossard, A. C., and Wiegmann, W. (1985). *Phys. Rev. Lett.* **54,** 1306–1309.

Knox, W. H., Hirlimann, C., Miller, D. A. B., Shah, J., Chemla, D. S., and Shank, C. V. (1986). *Phys. Rev. Lett.* **56,** 1191–1193.

Lee, Y. C., and Lin, D. L. (1979). *Phys. Rev. B* **19,** 1982–1989.
Liebler, J. G., Schmitt-Rink, S., and Haug, H. (1985). *J. Lumin.* **34,** 1–7.
Löwenau, J. P., Schmitt-Rink, S., and Haug, H. (1982). *Phys. Rev. Lett.* **49,** 1511–1514.
Masumoto, Y., Tarucha, S., and Okamoto, H. (1986). *J. Phys. Soc. Japan* **55,** 57–60.
Miller, D. A. B., Chemla, D. S., Smith, P. W., Gossard, A. C., and Wiegmann, W. (1982a). *Appl. Phys. B* **28,** 96–97.
Miller, D. A. B., Chemla, D. S., Eilenberger, D. J., Smith, P. W., Gossard, A. C., and Tsang, W. T. (1982b). *Appl. Phys. Lett.* **41,** 679–681.
Miller, D. A. B., Chemla, D. S., Eilenberger, D. J., Smith, P. W., Gossard, A. C., and Wiegmann, W. (1983a). *Appl. Phys. Lett.* **42,** 925–927.
Miller, D. A. B., Chemla, D. S., Smith, P. W., Gossard, A. C., and Wiegmann, W. (1983b). *Opt. Lett.* **8,** 477–479.
Miller, D. A. B., Chemla, D. S., Damen, T. C., Gossard, A. C., Wiegmann, W., Wood, T. H., and Burrus, C. A. (1985). *Phys. Rev. B* **32,** 1043–1060.
Miller, D. A. B., Chemla, D. S., and Schmitt-Rink, S. (1986a). *Phys. Rev. B* **33,** 6976–6982.
Miller, D. A. B., Weiner, J. S., and Chemla, D. S. (1986b). *IEEE J. Quantum Electron.* **QE-22,** 1816–1830.
Miller, R. C., and Kleinman, D. A. (1985). *J. Lumin.* **30,** 520–540.
Miller, R. C., Kleinman, D. A., Tsang, W. T., and Gossard, A. C. (1981). *Phys. Rev. B* **24,** 1134–1136.
Mollow, B. R. (1969). *Phys. Rev.* **188,** 1969–1975.
Mollow, B. R. (1972). *Phys. Rev. A* **5,** 2217–2222.
Mysyrowicz, A., Hulin, D., Antonetti, A., Migus, A., Masselink, W. T., and Morkoc, H. (1986). *Phys. Rev. Lett.* **56,** 2748–2751.
Nozieres, P., and Comte, C. (1982). *J. Physique* **43,** 1083–1098.
Peyghambarian, N., and Gibbs, H. M. (1985). *J. Opt. Soc. Am. B* **2,** 1215–1227.
Peyghambarian, N., Gibbs, H. M., Jewell, J. L., Antonetti, A., Migus, A., Hulin, D., and Mysyrowicz, A. (1984). *Phys. Rev. Lett.* **53,** 2433–2436.
Ruckenstein, A. E., Schmitt-Rink, S., and Miller, R. C. (1986). *Phys. Rev. Lett.* **56,** 504–507.
Schaefer, W., and Treusch, J. (1986). *Z. Phys. B* **63,** 407–426.
Schmitt-Rink, S. (1986). "Theory of Transient Excitonic Nonlinearities in Quantum Wells." *Proc. NSF Workshop on Optical Nonlinearities, Fast Phenomena and Signal Processing,* Tucson.
Schmitt-Rink, S., and Chemla, D. S. (1986). *Phys. Rev. Lett.* **57,** 2752–2755.
Schmitt-Rink, S., and Ell, C. (1985). *J. Lumin.* **30,** 585–596.
Schmitt-Rink, S., Chemla, D. S., and Miller, D. A. B. (1985). *Phys. Rev. B* **32,** 6601–6609.
Schmitt-Rink, S., Ell, C., Koch, S. W., Schmidt, H. E., and Haug, H. (1984). *Solid State Commun.* **52,** 123–125.
Schmitt-Rink, S., Ell, C., and Haug, H. (1986). *Phys. Rev. B* **33,** 1183–1189.
Segall, B. (1966). *Phys. Rev.* **150,** 734–747.
Shen, Y. R. (1984). *The Principle of Nonlinear Optics.* J. Wiley, New York.
Shinada, S., and Sugano, S. (1966). *J. Phys. Soc. Japan* **21,** 1936–1946.

Smith, P. W., Silberberg, Y., and Miller, D. A. B. (1985). *J. Opt. Soc. Am. B* **2,** 1228–1236.

Sooryakumar, R., Chemla, D. S., Pinczuk, A., Gossard, A., Wiegmann, W., and Sham, L. J. (1985). *Solid State Commun.* **54,** 859–862.

Sturge, M. D. (1962). *Phys. Rev.* **127,** 768–773.

Tai, K., Jewell, J. L., Tsang, W. T., Temkin, H., Panish, M., and Twu, Y. (1987a). *Appl. Phys. Lett.* **51,** 152 (1987).

Tai, K., Tsang, W. T., and Hegarty, J. (1987b). *Appl. Phys. Lett.* **51,** 86 (1987).

Takagahara, T., and Hanamura, E. (1986). *Phys. Rev. Lett.* **56,** 2533–2536.

Totsuji, H. (1975). *J. Phys. Soc. Japan* **39,** 253–254.

Von Lehmen, A., Zucker, J. E., Heritage, J. P., Chemla, D. S., and Gossard, A. C. (1986a). *Appl. Phys. Lett.* **48,** 1479–1481.

Von Lehmen, A., Chemla, D. S., Zucker, J. E., and Heritage, J. P. (1986b). *Opt. Lett.* **11,** 609–611.

Von Lehmen, A., Zucker, J. E., Heritage, J. P., and Chemla, D. S. (1987). *Phys. Rev. B* **35,** 6479–6482.

Watanabe, K., Karasawa, T., Komatsu, T., and Kaifu, Y. (1986). *J. Phys. Soc. Japan* **55,** 897–907.

Weiner, J. S., Chemla, D. S., Miller, D. A. B., Wood, T. H., Sivco, D., and Cho, A. Y. (1985a). *Appl. Phys. Lett.* **46,** 619–621.

Weiner, J. S., Chemla, D. S., Miller, D. A. B., Haus, H. A., Gossard, A. C., Wiegmann, W., and Burrus, C. A. (1985b). *Appl. Phys. Lett.* **47,** 664–667.

Weisbuch, C., Dingle, R., Gossard, A. C., and Wiegmann, W. (1981). *Solid State Commun.* **38,** 709–712.

Zucker, J. E., Pinczuk, A., Chemla, D. S., Gossard, A. C., and Wiegmann, W. (1983). *Phys. Rev. Lett.* **51,** 1293–1296.

Zucker, J. E., Pinczuk, A., Chemla, D. S., Gossard, A. C., and Wiegmann, W. (1984a). *Phys. Rev. Lett.* **53,** 1280–1283.

Zucker, J. E., Pinczuk, A., Chemla, D. S., Gossard, A. C., and Weigmann, W. (1984b). *Phys. Rev. B* **29,** 7065–7068.

Zucker, J. E., Pinczuk, A., Chemla, D. S., and Gossard, A. C. (1987). *Phys. Rev. B* **35,** 2892–2895.